

Research Article

Applications of Steel Slag Powder and Steel Slag Aggregate in Ultra-High Performance Concrete

Jin Liu and Runhua Guo 

Department of Civil Engineering, Tsinghua University, Beijing 100084, China

Correspondence should be addressed to Runhua Guo; guorh@tsinghua.edu.cn

Received 21 October 2017; Accepted 19 November 2017; Published 30 January 2018

Academic Editor: Peng Zhang

Copyright © 2018 Jin Liu and Runhua Guo. This is an open access article distributed under the Creative Commons Attribution License, which permits unrestricted use, distribution, and reproduction in any medium, provided the original work is properly cited.

The applications of steel slag powder and steel slag aggregate in ultra-high performance concrete (UHPC) were investigated by determining the fluidity, nonevaporable water content, and pore structure of paste and the compressive strength of concrete and by observing the morphologies of hardened paste and the concrete fracture surface. The results show that the fluidity of the paste containing steel slag is higher. The nonevaporable water content of the hardened paste containing steel slag powder is close to that of the control sample at late ages. Both steel slag powder and steel slag aggregate react and connect tightly to gels and hardened paste, respectively. When the cement replacement ratio is no more than 10%, the proportion of pores larger than 50 nm in the hardened paste containing steel slag powder is close to that of the control sample, and the UHPC containing steel slag powder can display satisfactory compressive strengths. The UHPC containing steel slag aggregate demonstrates higher compressive strengths.

1. Introduction

Steel slag is a by-product of steel manufacturing [1]. Approximately 160 kg of steel slag is generated per ton of steel produced [2]. The common chemical compounds in steel slag are SiO_2 , CaO , Fe_2O_3 , Al_2O_3 , and MnO [3, 4]. The major mineral components of steel slag are C_3S , C_2S , C_4AF , RO phase, and free- CaO [5, 6]. Many studies have shown that steel slag can be applied in ceramics, road pavement materials, and other materials [7–9]. However, in some countries, a large amount of steel slag is still stockpiled without full utilization [10, 11].

The application of steel slag powder as a mineral admixture in concrete has been investigated in many studies [12–14]. Steel slag powder has hydraulic properties, and its hydration process is similar to that of cement [15, 16]. Studies have shown that concrete that contains steel slag powder performs better in terms of workability than plain cement concrete does [17]. The early autogenous shrinkage and adiabatic temperature rise of the concrete containing steel slag powder are also lower than those of concrete without steel slag powder [18, 19]. Additionally, the nonevaporable water content of the hardened paste containing fine steel slag

powder is close to that of hardened plain cement paste at late ages [20, 21]. Due to the negative influence of steel slag powder on the compressive strength, the chloride-ion penetration resistance, carbonation resistance, and sulfate-attack resistance of concrete, the cement replacement ratio should not be very high [21–23].

Research has also shown that steel slag could be used as either a coarse or fine aggregate for concrete [24–26]. The physical properties of steel slag aggregate are better than those of crushed limestone aggregate [27]. Due to the high density of steel slag, concrete containing steel slag aggregate has a higher density than plain cement concrete does [28]. In addition, concrete containing steel slag aggregate displays satisfactory compressive strengths and flexural strengths [28–30].

Ultra-high performance concrete (UHPC) is a new type of cement-based material. In general, UHPC consists of cement, silica fume, quartz sand, fiber, superplasticizer, and other constituents and exhibits very high compressive strength, high ductility, and outstanding durability [31–35]. High-temperature curing is usually used for UHPC, which is beneficial for the early hydration of cement and mineral admixtures [36–38]. The applications of many kinds of

industrial by-products, such as ground-granulated blast furnace slag, phosphorus slag, fly ash, and copper slag, in UHPC have been reported [39–42]. However, few studies have investigated the application of steel slag in UHPC. In this paper, the applications of steel slag as mineral admixture and aggregate in UHPC were discussed.

2. Raw Materials and Test Methods

2.1. Raw Materials. The cement used was ordinary Portland cement, which complies with the Chinese National Standard GB175-2007. The specific surface area and strength grade of the cement were $350 \text{ m}^2\text{kg}^{-1}$ and 42.5, respectively. The steel slag used was the converter steel slag with 1.5% $f\text{-CaO}$ (by mass). Figure 1 shows the particle size distributions of the cement and steel slag powder. The X-ray diffraction (XRD) patterns of the steel slag are shown in Figure 2. The major chemical components of the cement and steel slag are shown in Table 1. Table 2 provides the major chemical components of the silica fume.

The fine aggregate used was quartz sand with 98.2% SiO_2 (by mass). The quartz sands were classified into three levels: coarse quartz sand, medium quartz sand, and fine quartz sand. The diameters of coarse quartz sand, medium quartz sand, and fine quartz sand ranged from 0.63 to 1.25 mm, 0.315 to 0.63 mm, and 0.16 to 0.315 mm, respectively. The steel slag aggregate diameter range was the same as that of coarse quartz sand. Figure 3 shows the photo of the steel slag aggregate and coarse quartz sand.

The diameter and length of the steel fiber used ranged from 0.18 to 0.23 mm and 12 to 14 mm, respectively. The tensile strength of the steel fiber was more than 2850 MPa. Polycarboxylate superplasticizer (SP) with a solid content of 35% (by mass) was used to regulate the fluidity of the concrete.

2.2. Test Methods. Tables 3 and 4 list the mix proportions of the concretes and pastes, respectively. The water-to-binder ratio of the concretes and pastes is 0.16. The raw materials for the concretes were prepared in the following order. First, the aggregate (quartz sand and steel slag aggregate) and steel fiber were mixed and stirred for 4 minutes. Then, cement and silica fume were added and stirred for 2 minutes. Finally, water and superplasticizer were added, and the mixture was stirred until it was cast.

In order to accelerate the hydration degree of cement and mineral admixtures at early ages, a high-temperature curing method was used in this study. After casting, the concretes were kept at environmental temperature for 6 h. Then, they were cured at $40 \pm 5^\circ\text{C}$ with a relative humidity of more than 85% for 24 h. Subsequently, the concretes were released from molds and cured at $70 \pm 5^\circ\text{C}$ with a relative humidity of more than 95% for 48 h. After high-temperature curing, the concretes were cooled to room temperature. The heating and cooling rates were less than 15°C/h and 20°C/h , respectively. Finally, the concretes were watered and cured under a plastic film cover until 28 d.

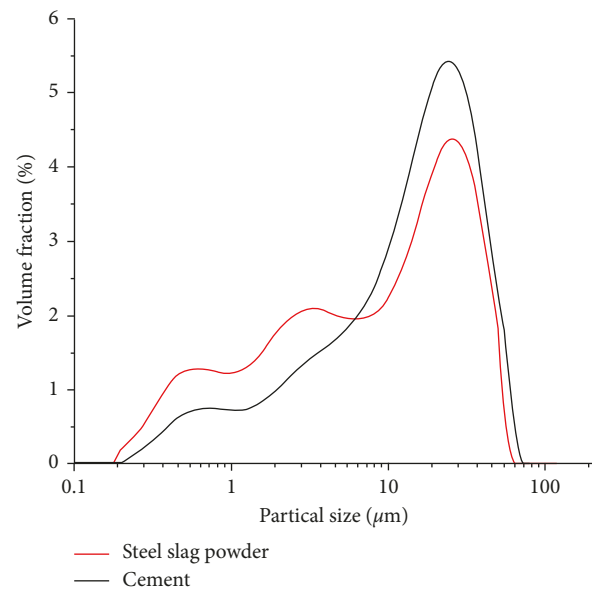


FIGURE 1: The particle size distributions of the cement and steel slag powder.

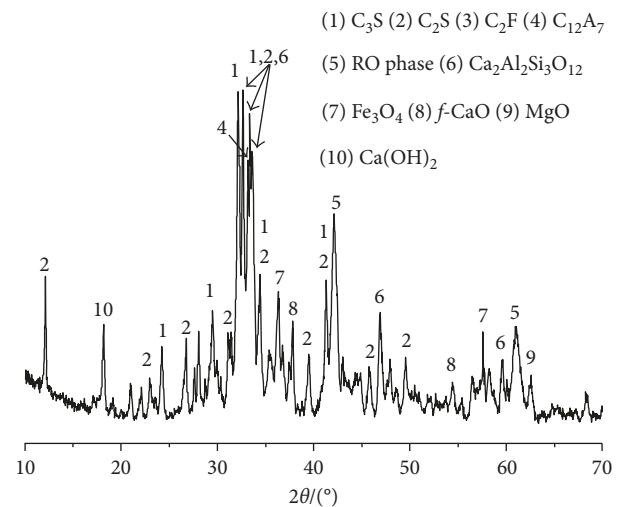


FIGURE 2: XRD patterns of the steel slag.

Concretes of $100 \times 100 \times 100 \text{ mm}$ were cast. A study of compressive strength was conducted according to Chinese National Standard GB/T50081-2002 with a loading rate of 1.2 MPa/s. Fluidity testing of the paste was conducted according to Chinese National Standard GB/T8077-2012. Pastes were cast in plastic sealed tubes to prevent both water loss and carbonation, and they were cured under the same conditions used with concretes. At testing ages, hardened pastes were extracted and then immersed in absolute alcohol to prevent further hydration. An electric vacuum-drying oven was used to dry the samples before testing. At the age of 28 d, a mercury intrusion porosimeter (MIP) was used to determine the pore characteristics of the hardened pastes. At the age of 28 d, the morphologies of the hardened paste and the concrete fracture surface were observed using scanning

TABLE 1: Chemical compositions of the cement and steel slag (%).

Sample	SiO ₂	Al ₂ O ₃	Fe ₂ O ₃	CaO	MgO	MnO	P ₂ O ₅	SO ₃	Na ₂ O _{eq}	Loss
Cement	22.36	7.73	3.66	57.21	3.10	—	—	3.54	0.73	2.31
Steel slag	19.11	7.46	18.01	43.37	5.17	2.66	1.76	—	0.41	1.36

$$\text{Na}_2\text{O}_{\text{eq}} = \text{Na}_2\text{O} + 0.685\text{K}_2\text{O}.$$

TABLE 2: Chemical compositions of the silica fumes (%).

Sample	SiO ₂	K	Na	H ₂ O	Loss
Silica fume	92.30	0.06	0.02	1.1	2.5



FIGURE 3: Photo of steel slag aggregate and coarse quartz sand.

electron microscopy (SEM). Energy-dispersive X-ray (EDX) was used to detect the elemental distributions of the hardened pastes and aggregates. The nonevaporable water (w_n) content of hardened paste was obtained from the mass difference between the sample dried at 105°C and heated at 1000°C normalized by the mass after only being dried at 105°C and correcting for the loss from the ignition of the unhydrated sample.

3. Results and Discussion

3.1. Fluidity. Figure 4 shows the fluidity of the pastes. Due to the very low water-to-binder ratio and the high water absorption of silica fume, the fluidity of the paste without steel slag powder is relatively low. However, the fluidity of the paste increases with the cement replacement ratio. When the cement replacement ratio is 20%, the fluidity of paste containing steel slag powder is approximately 25 mm higher than that of paste without steel slag powder. These results indicate that using steel slag powder as a mineral admixture could improve the fluidity of paste, which is beneficial for the workability of concrete. This may be because that the activity of steel slag powder is lower than that of cement, and the water requirement of composite binder containing steel slag powder is less than that of the equal mass cement in the same plastic state. These results are consistent with a previous study [17].

3.2. Nonevaporable Water Content. The nonevaporable water content reflects the amount of hydration products of cement and mineral admixture. Figure 5 shows the

nonevaporable water content of hardened pastes at 3 d (the end of high-temperature curing) and 28 d. At 3 d, the nonevaporable water content of the hardened paste containing steel slag powder is obviously lower than that of the hardened paste PC. Additionally, the nonevaporable water content of the hardened paste containing steel slag powder decreases with the cement replacement ratio. These results indicate that the hydration activity of steel slag powder is lower than that of cement, which is consistent with previous researches [15, 16]. Due to the elevated hydration degree during the initial high-temperature curing process, the nonevaporable water content of the hardened paste PC does not increase dramatically from 3 d to 28 d. However, at 28 d, the nonevaporable water content of the hardened paste containing steel slag powder is close to that of the hardened paste PC, which means that the nonevaporable water content growth rate of the hardened paste containing steel slag powder is higher than that of hardened paste PC. These results indicate that steel slag powder has more continuous hydration activity than cement does at late ages.

3.3. SEM and EDX Results. Figures 6(a) and 6(b) show the SEM morphologies of hardened pastes PS3 and PS4 at 28 d, respectively. Figures 6(c) and 6(d) show the EDX spectrums of positions 1 and 2, respectively. As shown in Figures 6(a) and 6(b), some particles have not reacted completely in the microstructures of the hardened pastes PS3 and PS4. According to the EDX results, these particles are steel slag. A layer of hydration products has wrapped the steel slag particles. In addition, the steel slag particles connect tightly to the gel around them. The outlines of steel slag particles also cannot be distinguished clearly because C-S-H gels are produced during the hydration of steel slag powder [15-16]. Meanwhile, the hydration activity of steel slag powder is enhanced by early high-temperature curing, and the hydration degree of steel slag powder is already high at 28 d.

Figures 7(a) and 7(b) show the SEM morphologies of the fracture surfaces of concretes AS1 and AS2, respectively. Figures 7(c)–7(f) show the EDX spectra of positions 3, 4, 5, and 6, respectively. According to the EDX results and the morphology, the bulging parts in the upper left sections of Figures 7(a) and 7(b) are steel slag aggregates. The relatively low-lying zones on the lower right sections of Figures 7(a) and 7(b) are hardened pastes. As shown in Figures 7(a) and 7(b), some hydration products were produced at the surface of the steel slag aggregates, and the steel slag aggregates connect tightly with the hardened paste. In addition, the boundaries between steel slag aggregates and hardened pastes cannot be distinguished clearly. These results indicate that, similar to steel slag powder, steel slag aggregate has reacted to some extent and produced some hydration

TABLE 3: Mix proportions of concretes (kg/m³).

Samples	Cement	Steel slag powder	Silica fume	Steel slag aggregate	Quartz sand			Steel fiber	Water	SP
					Coarse	Medium	Fine			
C	810	0	150	0	300	750	150	130	120	52
S1	769.5	40.5	150	0	300	750	150	130	120	52
S2	729	81	150	0	300	750	150	130	120	52
S3	688.5	121.5	150	0	300	750	150	130	120	52
S4	648	162	150	0	300	750	150	130	120	52
AS1	810	0	150	150	150	750	150	130	120	52
AS2	810	0	150	300	0	750	150	130	120	52

TABLE 4: Mix proportions of pastes (g).

Samples	Cement	Steel slag powder	Silica fume	Water	SP
PC	100	0	18.5	15.8	4.9
PS1	95	5	18.5	15.8	4.9
PS2	90	10	18.5	15.8	4.9
PS3	85	15	18.5	15.8	4.9
PS4	80	20	18.5	15.8	4.9

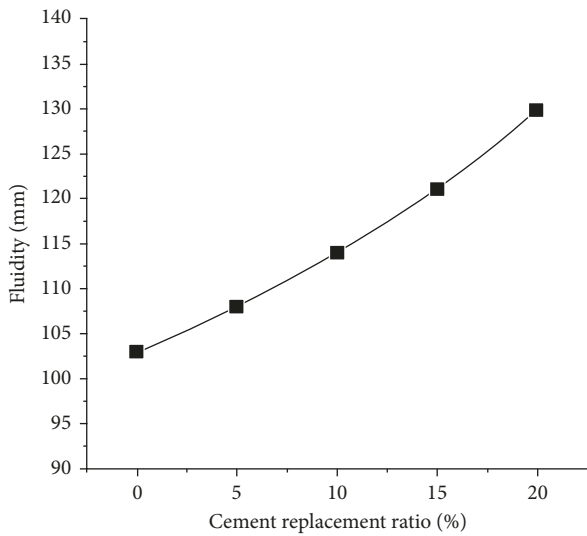


FIGURE 4: The fluidity of pastes.

products at 28 d, which is conducive to the connection of steel slag aggregate with the hardened paste. This may be attributed to the activating effect on the steel slag aggregate produced during the initial high-temperature curing.

3.4. Pore Structures. Figure 8 shows the pore structures of the hardened pastes at 28 d. Owing to the very low water-to-binder ratio, the pore structure of hardened paste PC is very fine. The cumulative pore volume of the hardened paste containing steel slag powder increases dramatically with the cement replacement ratio. This result is consistent with previous studies [21, 23]. It is noteworthy that although the cumulative pore volumes of hardened pastes PS1 and PS2 are higher than that of hardened paste PC, the proportions of pores larger than 50 nm in hardened pastes PS1 and PS2 are

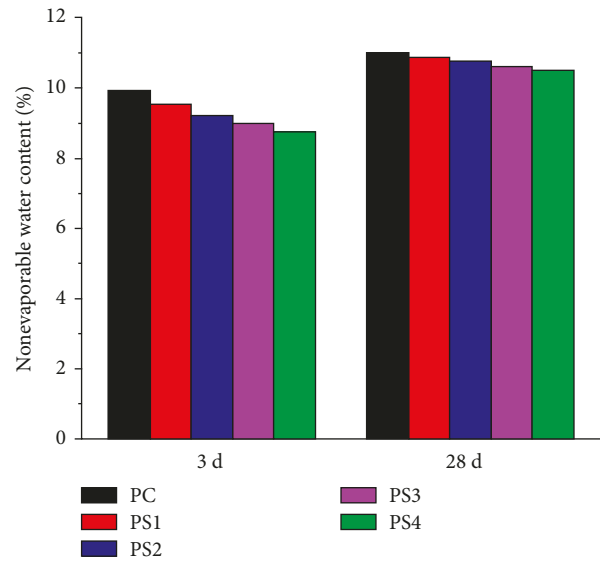


FIGURE 5: Nonevaporable water contents of hardened pastes.

close to that of hardened paste PC, which may be attributed to the high hydration degree of steel slag powder. However, when the cement replacement ratio is more than 10%, both the cumulative pore volume and the proportion of pores larger than 50 nm in the hardened paste containing steel slag powder are significantly higher than those in hardened paste PC.

3.5. Compressive Strength. Figure 9 shows the compressive strengths of the concretes at 28 d. The compressive strengths of concretes S2 and S3 are higher than 150 MPa and are very close to that of concrete C. This occurs because the proportions of pores larger than 50 nm in hardened pastes PS1 and PS2 are close to that in hardened paste PC; this proportion plays an important role in the compressive strength of concretes. However, the compressive strengths of concretes S3 and S4 are significantly lower than that of concrete C. This is because both the cumulative pore volumes and the proportions of pores larger than 50 nm in the hardened pastes PS3 and PS4 are significantly higher than those in hardened paste PC. Overall, when the cement replacement ratio is no more than 10%, the UHPC containing steel slag powder can display satisfactory compressive strength.

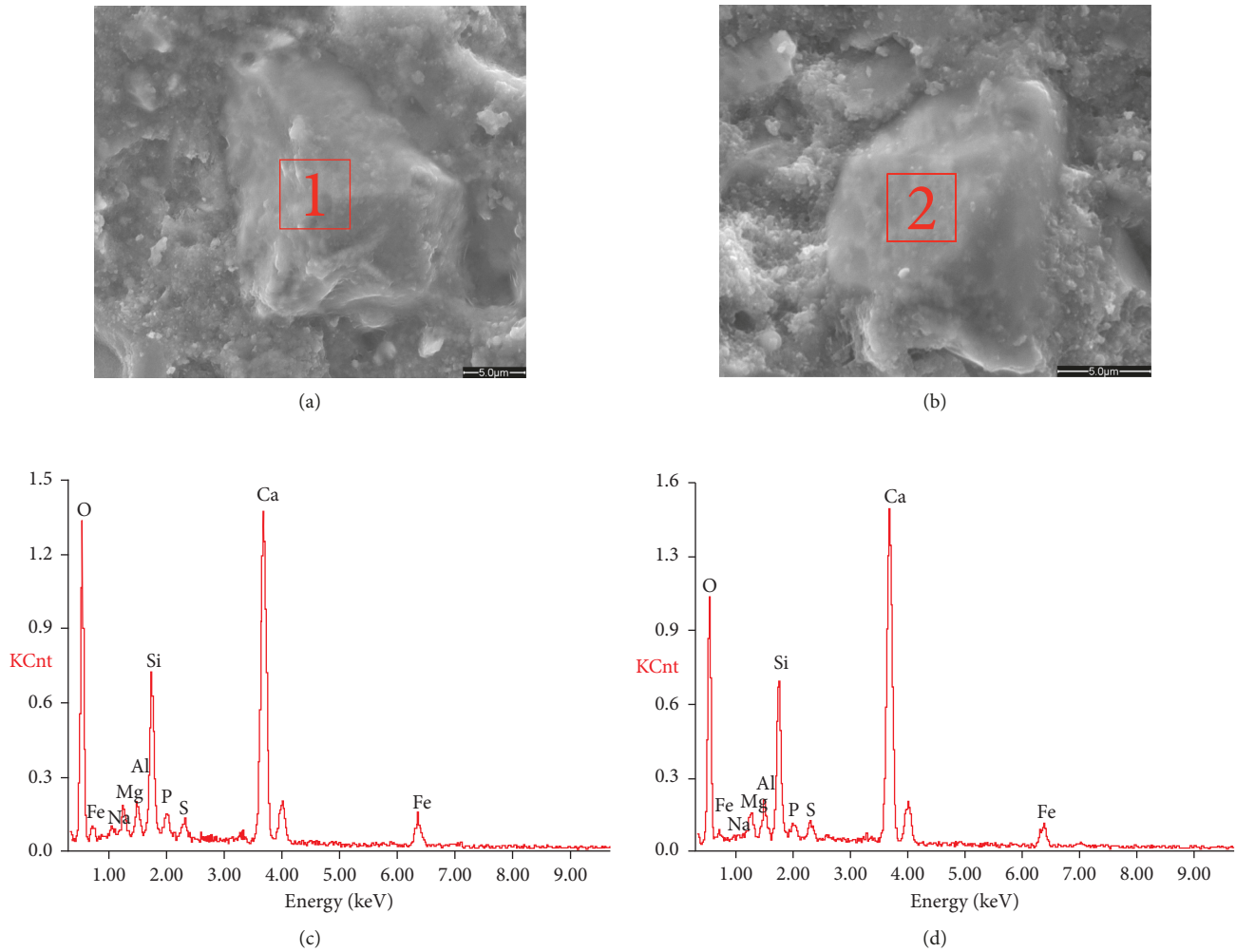


FIGURE 6: (a) SEM morphology of hardened paste PS3 at 28 d. (b) SEM morphology of hardened paste PS4 at 28 d. (c) EDX spectrum of position 1. (d) EDX spectrum of position 2.

The compressive strengths of concretes AS1 and AS2 are higher than that of concrete C. Meanwhile, the compressive strength of the concrete containing steel slag aggregate increases with the coarse quartz sand replacement ratio. This is because when the compressive strength of concrete is very high, the bonding condition between the aggregate and hardened paste plays a very important role in the compressive strength of concrete. In addition, according to the SEM and EDX results, steel slag aggregates react and connect with hardened paste tightly. Overall, the UHPC containing steel slag aggregate shows higher compressive strength.

4. Conclusions

- (1) Steel slag powder used as a mineral admixture could improve the fluidity of paste, which is beneficial for the workability of concrete.
- (2) When both are subjected to high-temperature curing conditions at early ages, steel slag powder has more continuous reaction activity than cement does at late

ages. The nonevaporable water content of the hardened paste containing steel slag powder is close to that of the control sample at late ages.

- (3) Under high-temperature curing conditions at early curing ages, hydraulic steel slag particles connect with the gel around them tightly. When the cement replacement ratio is no more than 10%, the proportion of pores larger than 50 nm in the hardened paste containing steel slag powder is close to that in the control sample, and the UHPC containing steel slag powder can display satisfactory compressive strength.
- (4) Under high-temperature curing conditions at early ages, the steel slag aggregate reacts and connects tightly with hardened paste. The UHPC containing steel slag aggregate shows higher compressive strengths.

Conflicts of Interest

The authors declare that there are no conflicts of interest regarding the publication of this paper.

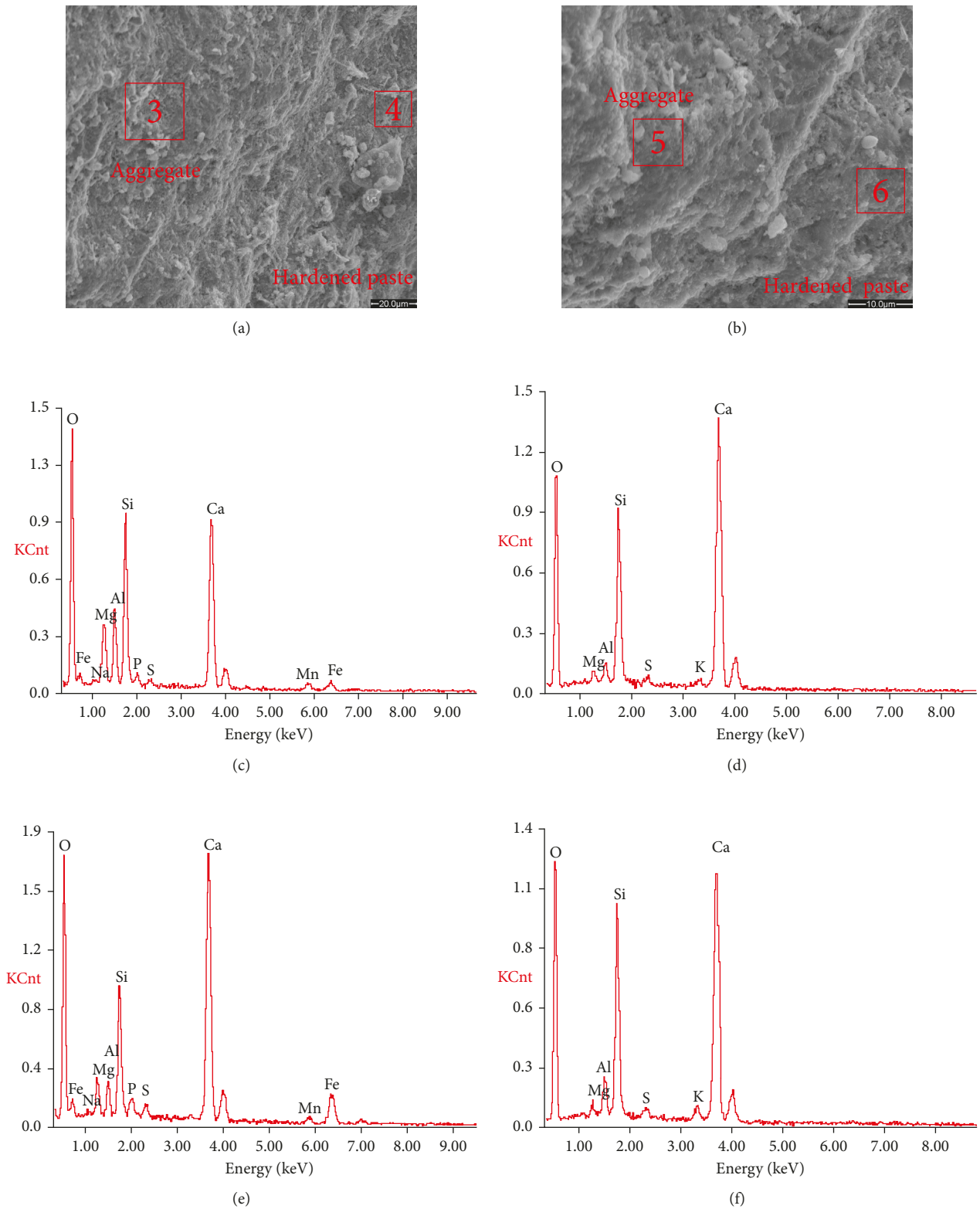


FIGURE 7: (a) SEM morphology of the fracture surface of concrete AS1 at 28 d. (b) SEM morphology of the fracture surface of concrete AS2 at 28 d. (c) EDX spectrum of position 3. (d) EDX spectrum of position 4. (e) EDX spectrum of position 5. (f) EDX spectrum of position 6.

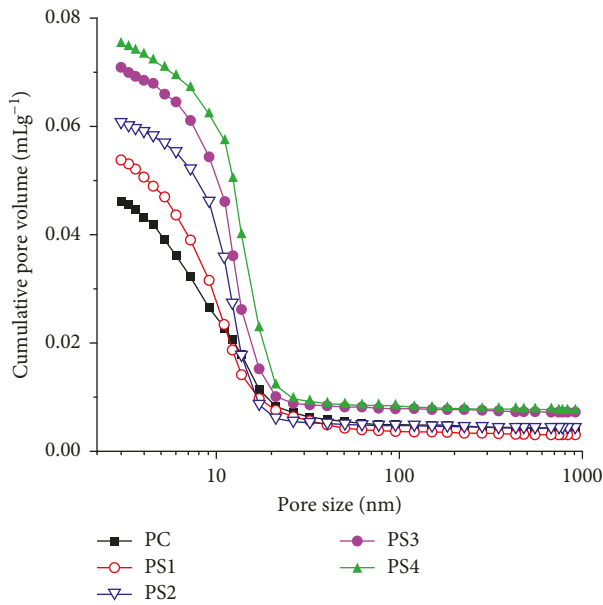


FIGURE 8: Pore structures of the hardened pastes at 28 d.

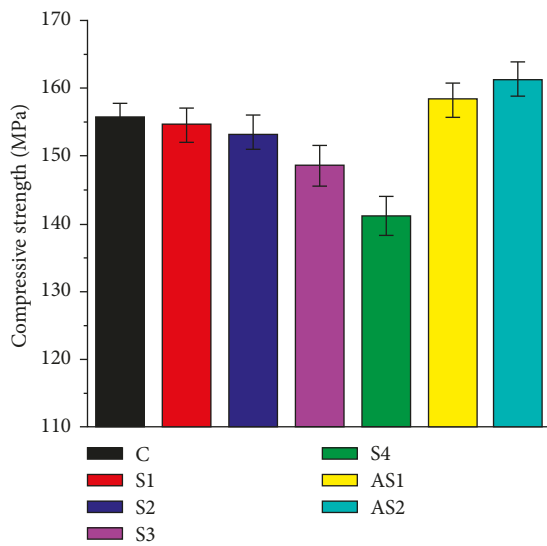


FIGURE 9: Compressive strengths of the concretes at 28 d.

References

- [1] C. Shi, "Steel slag-its production, processing, characteristics, and cementitious properties," *Journal of Materials in Civil Engineering*, vol. 16, no. 3, pp. 230–236, 2004.
- [2] E. Furlani, G. Tonello, and S. Maschio, "Recycling of steel slag and glass cullet from energy saving lamps by fast firing production of ceramics," *Waste Management*, vol. 30, no. 8-9, pp. 1714–1719, 2010.
- [3] M. Tufekci, A. Demirbas, and H. Genc, "Evaluation of steel furnace slags as cement additives," *Cement and Concrete Research*, vol. 27, no. 11, pp. 1713–1717, 1997.
- [4] T. S. Zhang, F. T. Liu, S. Q. Liu, Z. H. Zhou, and X. Cheng, "Factors influencing the properties of a steel slag composite cement," *Advances in Cement Research*, vol. 20, no. 4, pp. 145–150, 2008.
- [5] S. Kourounis, S. Tsivilis, P. E. Tsakiridis, G. D. Papadimitriou, and Z. Tsibouki, "Properties and hydration of blended cements with steelmaking slag," *Cement and Concrete Research*, vol. 37, no. 6, pp. 815–822, 2007.
- [6] T. Zhang, Q. Yu, J. Wei, J. Li, and P. Zhang, "Preparation of high performance blended cements and reclamation of iron concentrate from basic oxygen furnace steel slag," *Resources, Conservation and Recycling*, vol. 56, no. 1, pp. 48–55, 2011.
- [7] R. J. Galán-Arboledas, J. Á. D. Diego, M. Dondi, and S. Bueno, "Energy, environmental and technical assessment for the incorporation of EAF stainless steel slag in ceramic building materials," *Journal of Cleaner Production*, vol. 142, pp. 1778–1788, 2017.
- [8] L. D. Poulidakos, C. Papadaskalopoulou, B. Hofko et al., "Harvesting the unexplored potential of European waste materials for road construction. Resources," *Conservation and Recycling*, vol. 116, pp. 32–44, 2017.
- [9] M. Pasetto, A. Baliello, G. Giacomello, and E. Pasquini, "Sustainable solutions for road pavements: a multi-scale characterization of warm mix asphalts containing steel slags," *Journal of Cleaner Production*, vol. 166, pp. 835–843, 2017.
- [10] P. Sun and Z. C. Guo, "Sintering preparation of porous sound-absorbing materials from steel slag," *Transactions of Non-ferrous Metals Society of China*, vol. 25, no. 7, pp. 2230–2240, 2015.
- [11] İ. Yüksel, "A review of steel slag usage in construction industry for sustainable development," *Environment Development and Sustainability*, vol. 19, no. 2, pp. 369–384, 2017.
- [12] Q. Wang, D. Wang, and S. Zhuang, "The soundness of steel slag with different free CaO and MgO contents," *Construction and Building Materials*, vol. 151, pp. 138–146, 2017.
- [13] J. Liu and D. Wang, "Influence of steel slag-silica fume composite mineral admixture on the properties of concrete," *Powder Technology*, vol. 320, pp. 230–238, 2017.
- [14] J. Liu and D. Wang, "Application of ground granulate blast furnace slag-steel slag composite binder in a massive concrete structure under severe sulphate attack," *Advances in Materials Science and Engineering*, vol. 2017, Article ID 9493043, 9 pages, 2017.
- [15] J. Li, Q. Yu, J. Wei, and T. Zhang, "Structural characteristics and hydration kinetics of modified steel slag," *Cement and Concrete Research*, vol. 41, no. 3, pp. 324–329, 2011.
- [16] S. Liu, Q. Li, G. Xie, L. Li, and H. Xiao, "Effect of grinding time on the particle characteristics of glass powder," *Powder Technology*, vol. 295, pp. 133–141, 2016.
- [17] Y.-C. Peng and C.-L. Hwang, "Carbon steel slag as cementitious material for self-consolidating concrete," *Journal of Zhejiang University-Science A*, vol. 11, no. 7, pp. 488–494, 2010.
- [18] W. Qiang, S. Mengxiao, and Y. Jun, "Influence of classified steel slag with particle sizes smaller than 20 μm on the properties of cement and concrete," *Construction and Building Materials*, vol. 123, pp. 601–610, 2016.
- [19] M. Shi, Q. Wang, and Z. Zhou, "Comparison of the properties between high-volume fly ash concrete and high-volume steel slag concrete under temperature matching curing condition," *Construction and Building Materials*, vol. 98, pp. 649–655, 2015.
- [20] S. Liu and L. Li, "Influence of fineness on the cementitious properties of steel slag," *Journal of Thermal Analysis and Calorimetry*, vol. 117, no. 2, pp. 629–634, 2014.
- [21] Q. Wang, J. Yang, and P. Yan, "Cementitious properties of super-fine steel slag," *Powder Technology*, vol. 245, pp. 35–39, 2013.

- [22] T. Zhang, Q. Yu, J. Wei, and J. Li, "Investigation on mechanical properties, durability and micro-structural development of steel slag blended cements," *Journal of Thermal Analysis and Calorimetry*, vol. 110, no. 2, pp. 633–639, 2012.
- [23] J. Hu, "Comparison between the effects of superfine steel slag and superfine phosphorus slag on the long-term performances and durability of concrete," *Journal of Thermal Analysis and Calorimetry*, vol. 128, no. 3, pp. 1251–1263, 2017.
- [24] L. Mo, F. Zhang, M. Deng, F. Jin, A. Al-Tabbaa, and A. Wang, "Accelerated carbonation and performance of concrete made with steel slag as binding materials and aggregates," *Cement and Concrete Composites*, vol. 83, pp. 138–145, 2017.
- [25] I. Netinger, D. Varevac, D. Bjegović, and D. Morić, "Effect of high temperature on properties of steel slag aggregate concrete," *Fire Safety Journal*, vol. 59, pp. 1–7, 2013.
- [26] N. Palankar, A. U. Ravi Shankar, and B. M. Mithun, "Durability studies on eco-friendly concrete mixes incorporating steel slag as coarse aggregates," *Journal of Cleaner Production*, vol. 129, pp. 437–448, 2016.
- [27] M. Maslehuddin, M. Sharif Alfarabi, M. Shameem, M. Ibrahim, and M. S. Barry, "Comparison of properties of steel slag and crushed limestone aggregate concretes," *Construction and Building Materials*, vol. 17, no. 2, pp. 105–112, 2003.
- [28] Y. Biskri, D. Achoura, N. Chelghoum, and M. Mouret, "Mechanical and durability characteristics of High Performance Concrete containing steel slag and crystalized slag as aggregates," *Construction and Building Materials*, vol. 150, pp. 167–178, 2017.
- [29] S. Monosi, M. L. Ruello, and D. Sani, "Electric arc furnace slag as natural aggregate replacement in concrete production," *Cement and Concrete Composites*, vol. 66, pp. 66–72, 2016.
- [30] I. Netinger, D. Bjegović, and G. Vrhovac, "Utilisation of steel slag as an aggregate in concrete," *Materials and Structures*, vol. 44, no. 9, pp. 1565–1575, 2011.
- [31] M. Alkaysi and S. El-Tawil, "Effects of variations in the mix constituents of ultra high performance concrete (UHPC) on cost and performance," *Materials and Structures*, vol. 49, no. 10, pp. 4185–4200, 2016.
- [32] P. Zhang, Y.-N. Zhao, Q.-F. Li, T.-H. Zhang, and P. Wang, "Mechanical properties of fly ash concrete composite reinforced with nano-SiO₂ and steel fibre," *Current Science*, vol. 106, no. 11, pp. 1529–1537, 2014.
- [33] P. Zhang, Y.-N. Zhao, Q.-F. Li, P. Wang, and T.-H. Zhang, "Flexural toughness of steel fiber reinforced high performance concrete containing nano-SiO₂ and fly ash," *Scientific World Journal*, vol. 2014, Article ID 403743, 11 pages, 2014.
- [34] P. Smarzewski and D. Barnat-Hunek, "Effect of fiber hybridization on durability related properties of ultra-high performance concrete," *International Journal of Concrete Structures and Materials*, vol. 11, no. 2, pp. 315–325, 2017.
- [35] Z. Wenhua, Z. Yunsheng, and Z. Guorong, "Single and multiple dynamic impacts behaviour of ultra-high performance cementitious composite," *Journal of Wuhan University of Technology-Materials Science Edition*, vol. 26, no. 6, pp. 1227–1234, 2011.
- [36] J. Liu and D. Wang, "The role of phosphorus slag in steam-cured concrete," *Advances in Materials Science and Engineering*, vol. 2017, Article ID 8392435, 14 pages, 2017.
- [37] Z. Zhang, Q. Wang, and H. Chen, "Properties of high-volume limestone powder concrete under standard curing and steam-curing conditions," *Powder Technology*, vol. 301, pp. 16–25, 2016.
- [38] Q. Wang, D. Wang, and H. Chen, "The role of fly ash microsphere in the microstructure and macroscopic properties of high-strength concrete," *Cement and Concrete Composites*, vol. 83, pp. 125–137, 2017.
- [39] I. Ferdosian, A. Camões, and M. Ribeiro, "High-volume fly ash paste for developing ultra-high performance concrete (UHPC)," *Ciência & Tecnologia dos Materiais*, vol. 29, no. 1, pp. e157–e161, 2017.
- [40] R. S. Edwin, E. Gruyaert, and N. De Belie, "Influence of intensive vacuum mixing and heat treatment on compressive strength and microstructure of reactive powder concrete incorporating secondary copper slag as supplementary cementitious material," *Construction and Building Materials*, vol. 155, pp. 400–412, 2017.
- [41] H. Yazıcı, H. Yiğiter, A. Ş. Karabulut, and B. Baradan, "Utilization of fly ash and ground granulated blast furnace slag as an alternative silica source in reactive powder concrete," *Fuel*, vol. 87, no. 12, pp. 2401–2407, 2008.
- [42] P. Yanzhou, Z. Jun, L. Jiuyan, K. Jin, and W. Fazhou, "Properties and microstructure of reactive powder concrete having a high content of phosphorous slag powder and silica fume," *Construction and Building Materials*, vol. 101, pp. 482–487, 2015.



Hindawi

Submit your manuscripts at
www.hindawi.com

